Distribution of cations in wurtzitic $In_xGa_{1-x}N$ and $In_xAl_{1-x}N$ alloys: Consequences for energetics and quasiparticle electronic structures

Luiz Cláudio de Carvalho,[1,2,*] André Schleife,[1,2,3] Jürgen Furthmüller,[1,2] and Friedhelm Bechstedt[1,2]

[1]*Institut für Festkörpertheorie und -optik, Friedrich-Schiller-Universität, Max-Wien-Platz 1, D-07743 Jena, Germany*
[2]*European Theoretical Spectroscopy Facility (ETSF)*
[3]*Condensed Matter and Materials Division, Lawrence Livermore National Laboratory, Livermore, California 94550, USA*

The ternary, isostructural, wurtzite-derived group-III mononitride alloys $In_xGa_{1-x}N$ and $In_xAl_{1-x}N$ are reexamined within a cluster expansion approach. Using density functional theory together with the AM05 exchange-correlation functional, the total energies and the optimized atomic geometries of all 22 clusters classes of the cluster expansion for each material system are calculated. The computationally demanding calculation of the corresponding quasiparticle electronic structures is achieved for all cluster classes by means of a recently developed scheme to approximately solve the quasiparticle equation based on the HSE06 hybrid functional and the G_0W_0 approach. Using two different alloy statistics, the configurational averages for the lattice parameters, the mixing enthalpies, and the bulk moduli are calculated. The composition-dependent electronic structures of the alloys are discussed based on configurationally averaged electronic states, band gaps, and densities of states. Ordered cluster arrangements are found to be energetically rather unfavorable, however, they possess the smallest energy gaps and, hence, contribute to light emission. The influence of the alloy statistics on the composition dependencies and the corresponding bowing parameters of the band gaps is found to be significant and should, hence, lead to different signatures in the optical-absorption or -emission spectra.

I. INTRODUCTION

Group-III mononitride alloys such as $In_xGa_{1-x}N$ and $In_xAl_{1-x}N$ have attracted great interest due to their various applications in optoelectronics.[1] The development of the nitrides is largely driven by the advances in solid-state lighting, laser technology, and photovoltaics. One reason for that are the fundamental band gaps of the nitride alloys; they cover the electromagnetic spectrum from the infrared to the ultraviolet since the gaps of the binary nitrides are ≈0.7 eV (pure InN[2,3]), ≈3.5 eV (pure GaN[4]), and ≈6.2 eV (pure AlN[4]). Moreover, InN, GaN, and AlN crystallize in the wurtzite (wz) structure, hence, the energetically lowest optical transitions, that originate from the respective fundamental band gaps, are dipole-allowed and direct (i.e., they do not invoke phonons).

Unfortunately, despite the success in producing $In_xGa_{1-x}N$ laser diodes that operate at wave lengths of 400–450 nm, it is rather challenging to achieve lasing at more than 500 nm.[5] Increasing the emission wave length from ≈440 nm (blue) to ≈515 nm (green) requires an increase of the In molar fraction in the active $In_xGa_{1-x}N$ layers from about $x = 0.14$ to $x = 0.32$. However, the growth of defect-free and homogeneous $In_xGa_{1-x}N$ or $In_xAl_{1-x}N$ becomes more challenging for such large compositions x.[6] In some growth experiments [e.g., metal organic chemical vapor deposition (MOCVD)], the higher vapor pressure of InN with respect to that of GaN or AlN leads to low In incorporation into the alloys.[7] In addition, the difference of the formation enthalpies of InN and GaN/AlN causes a strong surface segregation of In.[8] Early studies[9,10] even suggested a solid phase miscibility gap due to the large differences of the bond lengths in InN and GaN/AlN.

In the literature, the main difficulty for the interpretation of the experimental results seems to be the definition of a characteristic length scale. Consequently, the atomic microstructure of the ternary III-nitride alloys is described using different wordings, somewhat depending on the method used for the structural investigations and also depending on the average composition of the alloy or the wz-$In_xGa_{1-x}N$ layers: *Alloy ordering* seems to occur in layers deposited by both MOCVD and molecular beam epitaxy.[11,12] In addition, *precipitation* or *phase separation*, which can in principle only be distinguished based on a characteristic length scale, have been observed.[12–14] Other composition inhomogeneities have been interpreted in terms of *compositional modulation*.[15,16] In addition, the reasons for inhomogeneities (i.e., if they are due to thermodynamics, growth kinetics, or layer deposition) often remain unclear.[6] In the more recent publications, such local variations in the composition are simply discussed as *composition fluctuation* on an nm-length scale[17,18] or are associated with *atomic condensates* (small spatial extent of <4 nm) of InN.[19]

The possible instability of $In_xX_{1-x}N$ (X = Ga, Al) against decomposition into two random alloys as well as the occurrence of fluctuations in a compositionally disordered system have been studied theoretically in a variety of papers.[10,20–26] Many of these studies[20–22] consistently predict a miscibility gap for $In_xGa_{1-x}N$ (mainly for the zinc-blende structure) in a broad temperature range and, hence, explain observations of precipitation or even spinodal decomposition.[27] More recently, minor component ordering and clustering in wz-$In_xGa_{1-x}N$ but also wz-$In_xAl_{1-x}N$ has been studied by means of multiscale or *ab initio* methods.[23–25]

Nevertheless, it has been found experimentally that the incorporation of small amounts of In leads to an enhancement of the light emission intensity in light-emitting diodes as well as laser diodes with respect to devices made from pure GaN or AlN.[28] This may be related to In clustering as well as composition fluctuations.[29] However, the short radiative lifetimes measured for alloys that contain In have also been

traced back to atomic condensates of In-N bonds.[30] This variety of results shows that a good grasp of the incorporation and distribution of In in the $In_xGa_{1-x}N$ or $In_xAl_{1-x}N$ alloys is crucial for both the device operation as well as the physical understanding of the material.

Ultimately, the local structural patterns of the alloy system determine its electronic properties.[24,25] Since the (optical) gap of an alloy can be measured by photoluminescence or optical absorption experiments, the majority of theoretical studies focused on the band gaps and, in particular, their nonlinear variation with the average composition x (see, e.g., Refs. 21,24,25,31–35). However, most of these electronic-structure studies rely on the density functional theory (DFT)[36,37] together with the local density approximation or the generalized-gradient approximation to describe exchange and correlation (XC). In these approximations the fundamental energy gap of a semiconductor is significantly underestimated[24,31–33] due to the missing quasiparticle (QP) effects.[38] Understanding the electronic structure and the optical properties of the alloys requires a more sophisticated approach,[39] for instance, most modern QP calculations.

Another limitation of most of the previous electronic-structure calculations is the use of just one atomic configuration to model an alloy with a given average composition x. Investigating only a certain fixed atomic geometry or an ordered structure cannot correctly describe the properties (clustering, ordering, composition fluctuation, etc.) of an alloy on an nm-scale. Hence, the corresponding results for alloy properties, such as the energy gap for a defined composition x, have a rather limited validity. Instead, the probability of the occurrence of such local structures has to be taken into account in a rigorous theoretical study; it is imperative to account for different configurations within a statistical scheme[40] (i.e., a certain alloy statistics has to be used).

The combination of various local configurations with an alloy statistics and the calculation of QP energies is a computational challenge which is possible nowadays.[39] In this paper, the alloy system is modeled by taking all possible combinations of In and Ga/Al atoms on the cation sublattice into account that arise when 16-atom cells with local wz geometry are assumed. For each of these clusters the equilibrium atomic geometry as well as the corresponding electronic structure is calculated and, subsequently, the respective alloy properties are computed as configurational averages. The theoretical and computational approaches are described in Sec. II. Results for thermodynamic and structural properties are given in Sec. III. In Sec. IV the electronic structures are discussed. Finally, in Sec. V, conclusions and a summary are given.

II. THEORETICAL AND COMPUTATIONAL METHODS

A. Cluster expansion and alloy statistics

The cluster expansion method[41,42] is one of the central approaches to describe isostructural ternary alloys. The version which is used in this work is described in detail in Refs. 21,40,43–45 and briefly outlined in the following.

For the cluster expansion, a macroscopic alloy $In_xX_{1-x}N$ is divided into M clusters, each of which consists of $2n$ atoms (n anions and n cations).[21,40,45] The entire alloy consists of
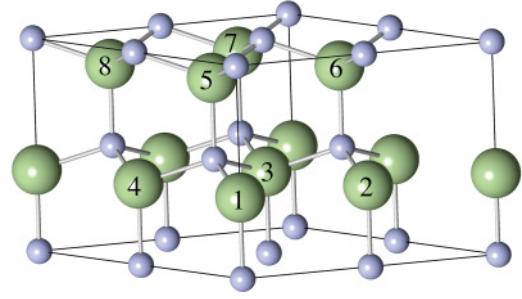

FIG. 1. (Color online) Illustration of atomic sites in the 16-atom clusters consisting of four wz cells. Anions (N atoms) are depicted as blue (small) balls, cations (In, Ga, or Al atoms, respectively) as green (large) balls with labels. The cell boundaries are indicated by thin solid lines.

$N = nM$ atoms on the anion sublattice and N atoms on the cation sublattice. Due to the symmetry of the crystal lattice, all possible $2n$-atom clusters can be grouped into $J + 1$ different classes. Each class j ($j = 0, ..., J$) comprises g_j clusters of the same total energy ε_j, where n_j denotes the number of In cations that belong to the class j. In this framework, any macroscopic alloy is built of a set of $\{M_0, M_1, ..., M_J\}$ clusters and a single class j contributes with its cluster fraction $x_j = M_j/M$. For these statistical weights x_j the relation $\Sigma_{j=0}^{J} x_j = 1$ holds.

The clusters for the nitride alloys in wz structure are modeled by 16-atom supercells (i.e., $n = 8$) as depicted in Fig. 1. Due to the point-group symmetry of wz, the total number of $2^n = 256$ clusters is grouped into $J + 1 = 22$ classes.[40,43] A complete treatment of all classes of larger clusters (e.g., of 32-atom clusters) with $n = 16$ would increase the CPU time too much because of the $2^n = 65\,536$ clusters needed to study. The 16-atom cell can be constructed in such a way that N atoms occupy the top and bottom surfaces of the cell (cf. Fig. 1). Since the N sublattice (although somewhat deformed after atomic relaxation) is present in all cluster materials, the clusters with such surfaces may roughly be considered to be statistically independent, at least in c-axis direction.

All classes j, except for the binary end components, represent more or less ordered systems along the three crystallographic directions $[11\bar{2}0]$, $[\bar{1}2\bar{1}0]$, and $[0001]$, giving rise to a and c planes in the unrelaxed starting geometries. Superlattices of ordered bilayers in $[0001]$ direction are of special interest; the most pronounced one is the class $j = 8$ with $In_4X_4N_8$ clusters. The cluster material consists of In-N and X-N bilayers with the axis parallel to $[0001]$. In the class $j = 12$, with $n_j = 4$ each cation layer consists of alternating rows of In and X atoms in each c plane in $[11\bar{2}0]$ direction.

B. Configurational average

Within the cluster-expansion framework any property P of the macroscopic alloy is connected to the respective properties P_j of the individual clusters via the Connolly-Williams formula,[21,46]

$$P(x,T) = \sum_{j=0}^{J} x_j(x,T)P_j. \qquad (1)$$

Fluctuations around the configurational averages can be described via the mean-square deviations,

$$\Delta P(x,T) = \sqrt{\sum_{j=0}^{J} x_j(x,T)P_j^2 - P^2(x,T)}. \qquad (2)$$

The weights $x_j(x,T)$ in Eqs. (1) and (2) depend on the average composition x of the alloy as well as the temperature T, hence, it is possible to account for the influence of different preparation conditions.[43] In this work, three situations are distinguished:

(i) The case of thermodynamic equilibrium is described by cluster fractions that lead to a minimum of the Helmholtz free energy $F(x,T)$. This is achieved within the so-called generalized quasichemical approximation (GQCA),[21,45] for which the weights are given by

$$x_j^{\mathrm{GQCA}}(x,T) = \frac{g_j \eta^{n_j} e^{-\beta \Delta \varepsilon_j}}{\sum_{j'=0}^{J} g_{j'} \eta^{n_{j'}} e^{-\beta \Delta \varepsilon_{j'}}}. \qquad (3)$$

Here $\beta = 1/k_B T$ and η is determined by minimizing $F(x,T)$ under the constraint $\Sigma_{j=0}^{J} n_j x_j = nx$.[21,43] The excess energy $\Delta \varepsilon_j$ of cluster j is defined with respect to the total energies of the binary end components ε_0 and ε_J as

$$\Delta \varepsilon_j = \varepsilon_j - \left(\frac{n_j}{n} \varepsilon_J + \frac{n - n_j}{n} \varepsilon_0 \right). \qquad (4)$$

(ii) Within the strict-regular solution (SRS) model[45] the ideal cluster fractions,

$$x_j^0(x) = g_j x^{n_j}(1-x)^{n-n_j}, \qquad (5)$$

are employed. They arise from a purely stochastic distribution of the clusters in the macroscopic alloy and are independent of the temperature as well as the clusters' excess energies. This case can be interpreted as the high-temperature limit of the GQCA.

(iii) The microscopic decomposition model (MDM) assumes that the cations of a certain type (In, Ga, or Al) are more likely to occur close to cations of the same type. This is realized by cluster fractions that only take the binary end components into account, that is,

$$x_j^{\mathrm{MDM}}(x) = \begin{cases} 1-x & \text{for} & j=0 \\ x & \text{for} & j=J \\ 0 & \text{otherwise} \end{cases}. \qquad (6)$$

Within the MDM, mixing does not lead to a gain of internal energy, which can be the case under certain preparation conditions. The MDM represents the low-temperature limit of the GQCA.

C. Bowing parameters

The dependence of an alloy property P on the average composition x can be related to the values of the property for the binary end components, $P(\mathrm{InN})$ and $P(\mathrm{XN})$, by introducing a bowing parameter $P_b(x)$ according to

$$P(x) = x P(\mathrm{InN}) + (1-x) P(\mathrm{XN}) - x(1-x) P_b(x). \qquad (7)$$

The most simple case, $P_b(x) \equiv 0$, is represented by the MDM in this work for which the variation with the composition is

linear. If P corresponds to lattice constants, this situation is known as Vegard's rule.[47]

For $P_b(x) \neq 0$ the property $P(x)$ in Eq. (7) shows a bowing as it is found, for instance, for the fundamental energy gaps. The parameter P_b itself may also depend on the average composition x. In this work the form,[48]

$$P_b(x) = P_{b,0}/(1 + P_{b,1} x^2), \qquad (8)$$

for the composition dependence is assumed and values for $P_{b,0}$ as well as $P_{b,1}$ are derived.

D. Total energy and cluster geometry

The ground-state properties of the clusters, such as total energies, structural parameters, and bulk moduli, are derived from DFT calculations based on the AM05 XC functional.[49] Explicit calculations are performed using the Vienna Ab-Initio Simulation Package (VASP)[50] and a plane-wave expansion of the Kohn-Sham (KS) states. The pseudopotentials are generated within the projector-augmented-wave method[51] that allows for the accurate treatment of the valence s and p electrons as well as of the In $4d$ and Ga $3d$ semicore states at moderate plane-wave cutoff energies of 400 eV. The Brillouin zones (BZs) of the 16-atom supercells are sampled using a $2 \times 2 \times 2$ Monkhorst-Pack **k**-point mesh.[52]

The equilibrium cell volume V and the isothermal bulk modulus B_0 (as well as its pressure derivative B_0') follow from fitting the total-energy curves $E(V)$ around their minima to the Murnaghan equation of state.[53] For each cluster geometry, the fully relaxed atomic positions are computed by ensuring that the Hellmann-Feynman forces are below 5 meV/Å. Subsequently, the lattice parameters c_j and a_j of the clusters in an effective wz structure are determined directly (c_j) or derived from the cell volume (a_j) after the cell shape has been relaxed.

E. Quasiparticle electronic structure

The KS eigenvalues obtained from DFT using the semilocal AM05 XC functional[49] cannot be identified with single-QP electronic excitation energies. To calculate those, typically, the QP equation,[38] which is derived from the Dyson equation of the many-body perturbation theory,[54] along with Hedin's GW approximation for the XC self-energy[38,55] is iteratively solved.

In this work, the wave functions and eigenvalues of a generalized KS equation[56] with a nonlocal XC potential derived from the HSE hybrid functional[57] is used[56,58] to obtain a good starting electronic structure for the calculation of QP energies within one step of perturbation theory. More specifically, HSE06[57] is employed with a range-separation parameter ω of 0.15 a.u.$^{-1}$ instead of $\omega = 0.11$ a.u.$^{-1}$, as suggested by Paier *et al.*[59,60] This approach is called HSE06+G_0W_0 method in the following; it leads to QP energies with a numerical accuracy of about 0.1 eV. To ensure converged results for the QP energies, the BZ is sampled by a $3 \times 3 \times 3$ **k**-point mesh.

The HSE06+G_0W_0 method, as described above, leads to direct fundamental gaps of $E_g = 6.31$ eV, 3.66 eV, and 0.64 eV for bulk wz-AlN, -GaN, and -InN, respectively.[61] In addition,
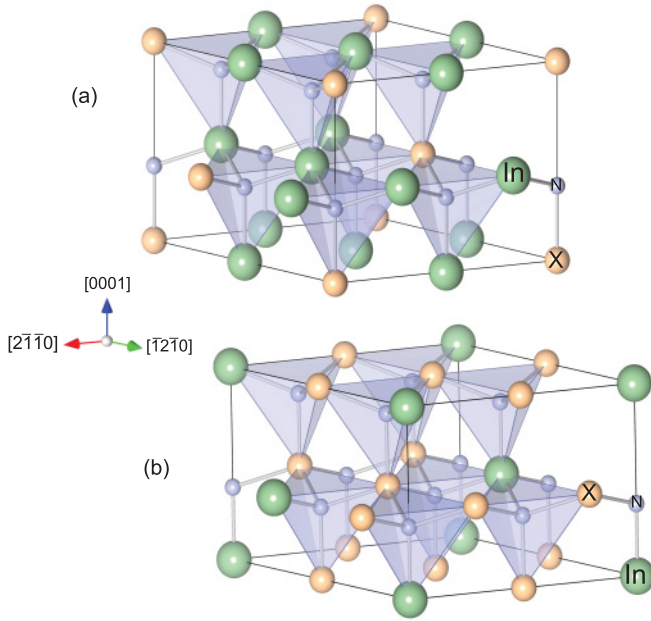
FIG. 2. (Color online) Ball-and-stick models for two cluster classes (a) $In_6X_2N_8$ ($j = 4$) and (b) $In_2X_6N_8$ ($j = 17$). The unit cell is indicated by black solid lines. The tetrahedra N-$In_i X_{4-i}$ (blue areas) that belong to the N atoms (small blue circles) in the unit cell are illustrated. The Cartesian axes **a**, **b**, and **c** correspond to the directions [11$\bar{2}$0], [$\bar{1}$2$\bar{1}$0], and [0001], respectively. Large green (medium yellow) circles represent In (Ga,Al) cations.

this scheme also yields binding energies of the Ga $3d$ and In $4d$ electrons not too far from experimental values.

III. THERMODYNAMIC AND STRUCTURAL PROPERTIES

A. Tendencies for clustering

While the tendencies for ordering and/or clustering in an alloy can intuitively be understood, it is, however, difficult to describe them quantitatively. It is also necessary to distinguish between short-range and long-range ordering. By means of the Warren-Cowley parameter,[62] the degree of short-range ordering in an alloy can be quantified and one can differentiate the atom distribution in a perfect random alloy from the clustered situation. The definition of this parameter can be easily applied to ternary systems based on zinc-blende crystals with 12 structurally equivalent second-nearest neighbor positions, as recently demonstrated for the ternary cubic nitrides.[25,63] Since the geometry is more difficult for wurtzitic systems with six second-nearest neighbors and two other cations in a slightly different distance, we introduce a different approach to characterize ordering in noncubic but tetrahedrally coordinated alloys.

First, for each of the eight N anions in a given cluster j, we count how many of the four *nearest neighbors* on the tetrahedral positions are In cations; this leads to five possible types of tetrahedra N-$In_i X_{4-i}$ with $i = \{0,1,2,3,4\}$ (see the two examples given in Fig. 2). By α_{ji} we denote the numbers of tetrahedra of type i that occur in the cluster class j for which

it holds $\alpha_{ji} = \{0,1,2,3,4,6,8\}$. It can be verified that the α_{ji} fulfill the relations,

$$\sum_{i=0}^{4} \alpha_{ji} = 8, \tag{9}$$

$$\frac{1}{4}\sum_{i=0}^{4} \alpha_{ji} \cdot i = n_j. \tag{10}$$

The first relation, Eq. (9), arises from the fact that there is a total of eight tetrahedra for each cluster cell. Equation (10) expresses that the total number of In atoms in cluster j equals n_j; the prefactor of $1/4$ ensures the correct counting of the In atoms. Note that the small perturbations of the ideal wz structure due to the relaxations of the atomic positions do *not* affect the assignment of the atoms to tetrahedra.

Second, based on the α_{ji} as introduced above, we define a parameter D_j which describes the tendency of clustering on an atomic length scale for the cations of the class j. D_j is defined as the averaged mean-square deviation of the number of In atoms in a given tetrahedron, i, from the number of In atoms per tetrahedron, $n_j/2$, that corresponds to a uniform distribution of In over the cation positions in the supercell. Due to the normalization to the total number of tetrahedra, Eq. (9), the quantity,

$$D_j = \frac{\sum_{i=0}^{4} \alpha_{ji}\left(i - \frac{1}{2}n_j\right)^2}{\sum_{i=0}^{4} \alpha_{ji}} = \frac{1}{8}\sum_{i=0}^{4}\alpha_{ji}\left(i - \frac{1}{2}n_j\right)^2, \tag{11}$$

varies in the interval $0 \leqslant D_j \leqslant 1$.

Table I contains the D_j values for the 22 cluster classes. The value $D_j = 0$ occurs for the binary end components and indicates a tendency for no clustering and uniform distribution. However, it is also found for the cluster classes $j = 4, 12, 17$ which contain only N-In_1X_3, N-In_2X_2, and N-In_3X_1 tetrahedra, respectively (i.e., only tetrahedra with $n_j/2$ In atoms are present in these cases). The maximum of $D_j = 1$ appears for the classes $j = 8,9,11$ with four In atoms. The classes $j = 8$ and 11 contain only tetrahedra of the type N-In_1X_3 and N-In_3X_1 and, hence, deviate from the uniform distribution of $n_j/2 = 2$. For $j = 9$, six N-In_2X_2 tetrahedra appear, which correspond to a uniform In distribution, however, the remaining two (N-In_4 and N-X_4) indicate strong clustering. Figure 3 clearly shows that the degree of clustering tends to maximum values for $n_j = 4$ and decreases toward $n_j = 0$ and $n_j = 8$. However, for a given n_j different D_j may occur (see Fig. 3).

The energetics of the clusters j with a given number of In atoms n_j seems to be clearly correlated to the tendency for clustering as described by D_j [cf. Eq. (11)]. The energetically most favored class $j = 12$ is characterized by $D_j = 0$ (no tendency for clustering), while the less favored one $j = 8$ leads to $D_j = 1$ (large tendency for clustering). More specifically, the maximum values of the excess energies of 20.0 meV/pair ($In_4Ga_4N_8$) or 29.4 meV/pair ($In_4Al_4N_8$) occur for the cluster class $j = 8$. This relation between energetics and tendency for clustering is also found for the classes $j = 4$ ($n_j = 2$) and $j = 17$ ($n_j = 6$). They are exclusively composed of N-In_1X_3 or N-In_3X_1 tetrahedra due to the alternating rows of X-X (or In-In) and X-In atom pairs in [11$\bar{2}$0] direction in both m and c planes. At the same time, they are the energetically most

TABLE I. Properties of the 22 cluster classes for In$_{n_j}$Ga$_{8-n_j}$N$_8$ (first line for each j) and In$_{n_j}$Al$_{8-n_j}$N$_8$ (second line for each j). Each class j is characterized by the number n_j of In atoms and the degeneracy g_j of the class. The degree D_j of the isotropic clustering (see text), the total energy per cation-anion pair ε_j (in eV/pair), the effective lattice constants c_j and a_j (in Å), the volume per cation-anion pair V_j (in Å^3/pair), and the bulk modulus $B_{0,j}$ (in GPa) are given for each j. In addition, the fundamental QP gap $E_{g,j}$ and the branch-point energy $E_{BP,j}$ with respect to the energy of the highest occupied state are listed.

class j	n_j	g_j	D_j	ε_j (eV/pair)	c_j (Å)	a_j (Å)	V_j (Å^3/pair)	$B_{0,j}$ (GPa)	$E_{g,j}$ (eV)	$E_{BP,j}$ (eV)
0	0	1	0.0	−12.503	5.17	3.18	22.66	184.2	3.571	2.358
				−14.877	4.97	3.12	20.94	200.6	6.328	3.409
1	1	8	0.25	−12.258	5.24	3.23	23.63	179.0	3.322	2.308
				−14.314	5.08	3.17	22.07	189.4	5.151	3.079
2	2	12	0.50	−12.019	5.31	3.26	24.62	169.0	2.580	2.122
				−13.760	5.19	3.20	23.28	180.6	3.999	2.550
3	2	12	0.50	−12.033	5.29	3.27	24.58	169.7	2.692	2.212
				−13.787	5.15	3.23	23.21	180.2	4.280	2.833
4	2	4	0.0	−12.052	5.31	3.27	24.58	170.9	2.684	2.192
				−13.815	5.19	3.21	23.20	181.6	4.441	2.916
5	3	8	0.75	−11.783	5.39	3.32	25.68	161.7	2.123	1.994
				−13.210	5.31	3.27	24.52	171.8	3.322	2.381
6	3	24	0.25	−11.831	5.37	3.31	25.58	162.7	2.243	2.065
				−13.291	5.27	3.26	24.37	174.1	3.525	2.523
7	3	24	0.75	−11.812	5.35	3.31	25.59	161.4	2.194	2.025
				−13.262	5.23	3.26	24.36	172.6	3.331	2.393
8	4	2	1.0	−11.550	5.49	3.36	26.43	151.4	1.644	1.814
				−12.661	5.44	3.31	25.87	156.5	2.571	2.049
9	4	8	1.0	−11.592	5.43	3.37	26.67	154.9	1.799	1.924
				−12.732	5.34	3.33	25.66	158.9	2.751	2.260
10	4	24	0.50	−11.612	5.44	3.36	26.66	155.6	1.803	1.919
				−12.764	5.37	3.32	25.65	162.2	2.813	2.274
11	4	6	1.0	−11.609	5.40	3.35	26.59	154.3	1.759	1.866
				−12.761	5.36	3.31	25.52	157.8	2.588	2.097
12	4	6	0.0	−11.647	5.44	3.34	26.59	157.1	1.857	1.946
				−12.823	5.37	3.30	25.56	163.0	2.986	2.399
13	4	24	0.50	−11.627	5.42	3.36	26.60	156.1	1.840	1.937
				−12.789	5.33	3.32	25.56	160.2	2.831	2.285
14	5	24	0.75	−11.411	5.48	3.40	27.65	150.4	1.431	1.791
				−12.283	5.41	3.37	26.85	152.9	2.147	2.021
15	5	24	0.25	−11.422	5.50	3.40	27.66	151.0	1.481	1.836
				−12.314	5.45	3.37	26.87	154.6	2.343	2.182
16	5	8	0.75	−11.392	5.53	3.41	27.78	147.9	1.381	1.777
				−12.233	5.49	3.37	27.05	152.4	2.123	1.993
17	6	4	0.0	−11.269	5.57	3.45	28.74	143.0	1.150	1.746
				−11.878	5.55	3.42	28.16	151.3	1.841	2.060
18	6	12	0.50	−11.249	5.55	3.46	28.72	141.0	1.168	1.727
				−11.827	5.50	3.43	28.13	149.1	1.682	1.918
19	6	12	0.50	−11.234	5.58	3.45	28.81	138.2	1.119	1.688
				−11.801	5.54	3.42	28.26	147.1	1.600	1.835
20	7	8	0.25	−11.075	5.65	3.50	29.96	129.9	0.737	1.587
				−11.360	5.61	3.49	29.58	137.0	1.119	1.735
21	8	1	0.0	−10.916	5.73	3.55	31.18	126.8	0.638	1.580

favorable ones of all classes j for the given $n_j = 2$ or 6 and are characterized by $D_j = 0$ (cf. Table I).

B. Energetics of the alloys

The total energies ε_j per cation-anion pair of the In$_{n_j}$Ga$_{8-n_j}$N$_8$ and In$_{n_j}$Al$_{8-n_j}$N$_8$ clusters in Table I show a monotonous decrease with the number n_j of the In cations. Figure 4 shows the excess energies [cf. Eq. (4)] and the mixing enthalpies (as the configurational averages of the excess energies). From this figure it becomes clear that the excess energies of InAlN are generally larger than those of InGaN with similar trends for the composition dependence for both alloys.
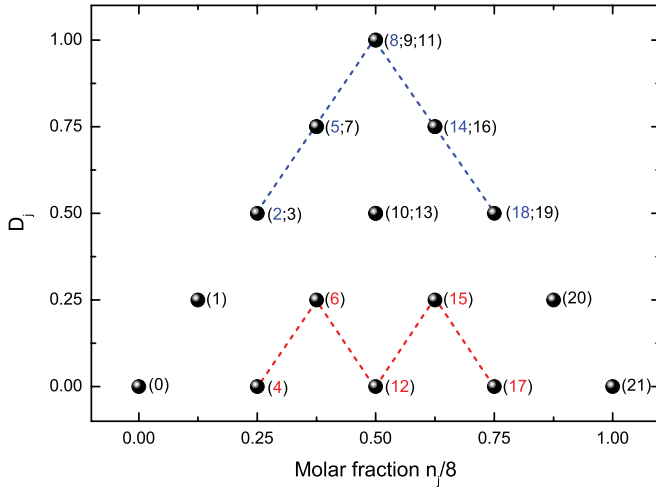
FIG. 3. (Color online) Degree of clustering D_j for all classes j (numbers given in parenthesis) of wz-$In_{n_j}X_{8-n_j}N_8$ versus the molar fraction $n_j/8$. The blue (red) dotted lines connect cluster classes j with lowest (highest) total energy per cation-anion pair.

In addition, as is common for isovalent and isostructural alloys, all excess energies and, hence, also the mixing enthalpies, are positive. This indicates that such alloys can be thermodynamically miscible only at temperatures T high enough for the entropy term $-T\Delta S$ (with ΔS being the mixing entropy) to be sufficiently negative.[26,45,64] Within the GQCA we computed critical temperatures for the miscibility of $T_c = 1914$ K at $x_c = 0.40$ for $In_xGa_{1-x}N$ and $T_c = 2610$ K at $x_c = 0.36$ for $In_xAl_{1-x}N$ in agreement with other more recent theoretical studies.[40,65] The different covalent radii can lead to different strains in the layers causing deviations from the homogeneity of the sublattice. According to Zunger and Mahajan,[66] this can also give rise to variations in the structural properties affecting the phase separation and/or the atomic ordering.
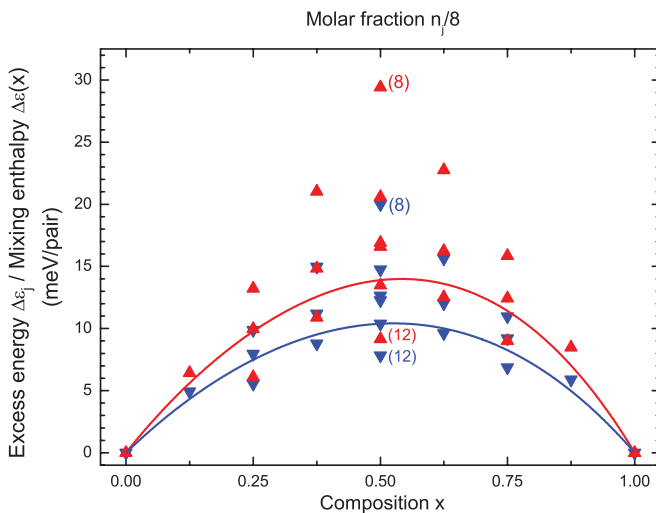
FIG. 4. (Color online) Excess energies $\Delta\varepsilon_j$ (triangles) and mixing enthalpies $\Delta\varepsilon(x)$ obtained using the SRS statistics (solid lines) versus fraction $n_j/8$ or composition x for InGaN (blue) and InAlN (red). The classes $j = 8$ ($j = 12$) are indicated.

C. Lattice parameters and bulk moduli

The optimization of the atomic coordinates in the $In_{n_j}Ga_{8-n_j}N_8$ and $In_{n_j}Al_{8-n_j}N_8$ cluster cells with an initial atomic geometry corresponding to four primitive wz unit cells (cf. Fig. 1) leads to the results compiled in Table I. From these results we calculate values of 12.9 % (11.0 %) and 14.2 % (10.3 %) for the mismatches of the a and c lattice parameters of binary InN and AlN (GaN). Our results are in good agreement with the experimental values[67–69] of 13.0 % (10.5 %) and 14.5 % (9.7 %), respectively, which shows that the internal local strain in the alloys due to the different In-N and Ga-N (Al-N) bond lengths is correctly described.

The configurational averages for the lattice parameters a and c, calculated using the SRS cluster statistics [cf. Eq. (5)] as well as the MDM [cf. Eq. (6)], are given in Fig. 5. As discussed above, the MDM results correspond to a linear interpolation between the binary end components (i.e., Vegard's rule[70] for a and c). The deviations of the SRS results from the straight MDM line are small. Consequently, Fig. 5 shows at first glance that Vegard's rule describes the situation fairly well. This has also been observed by other authors.[24,40]

More in detail, Vegard's rule is better fulfilled for the a lattice constant than for c in $In_xGa_{1-x}N$. The opposite is true for $In_xAl_{1-x}N$ where the c lattice constant varies nearly linearly with the composition x. These findings suggest to use $a(x)$ for $In_xGa_{1-x}N$ but $c(x)$ for $In_xAl_{1-x}N$ when determining the average composition x via Vegard's rule. Locally much stronger deviations from the linear interpolation as derived from Vegard's rule may occur; this is suggested by the lattice parameters of the individual cluster materials in Fig. 5.

In addition, as can be seen from Fig. 5, the bowing for alloys described within the SRS model is small. Note that the composition dependence of the lattice constant c for $In_xAl_{1-x}N$ shows a concave instead of a convex behavior. Assuming a composition-*independent* bowing [cf. Eq. (7)], we find $a_b = 0.021$ (0.064) Å and $c_b = 0.067$ (0.048) Å for $In_xGa_{1-x}N$ ($In_xAl_{1-x}N$). Taking the composition dependence of the bowing into account [cf. Eq. (8)] leads to values of $a_{b,0} = 0.022$ (0.063) Å, $a_{b,1} = 0.100$ (−0.073) and $c_{b,0} = 0.050$ (−0.117) Å, $c_{b,1} = -0.856$ (5.837) for $In_xGa_{1-x}N$ ($In_xAl_{1-x}N$). Even though the bowing is small for the composition dependence of the lattice constants, it may influence the determination of the average composition x using measured lattice parameters along with Vegard's rule. A maximum deviation of 0.02 Å from the linear interpolation leads to a maximum uncertainty of the composition of about 0.5 %.

The classes $j = 11,12$ for $In_4Ga_4N_8$ and $j = 8,12$ for $In_4Al_4N_8$ exhibit the strongest deviation from the linear interpolation: $c(x = 0.5) = 5.44 / 5.37$ Å and $a(x = 0.5) = 3.36 / 3.32$ Å, as computed from Table I. These classes are characterized by superlatticelike structures; the $j = 8$ material, for instance, consists of alternating c-plane bilayers in [0001] direction and in the case of the class $j = 11$ the superlattice is formed by m-plane bilayers in [1$\bar{1}$00] direction. Interestingly, both classes show the same high degree of clustering, $D_8 = D_{11} = 1$, with four tetrahedra of type N-In_3X_1 and four of type N-In_1X_3. It is noticeable that, in average, these classes show merely tetrahedra of type N-In_2X_2 as class $j = 12$ whose clustering degree is $D_{12} = 0$. It is likely

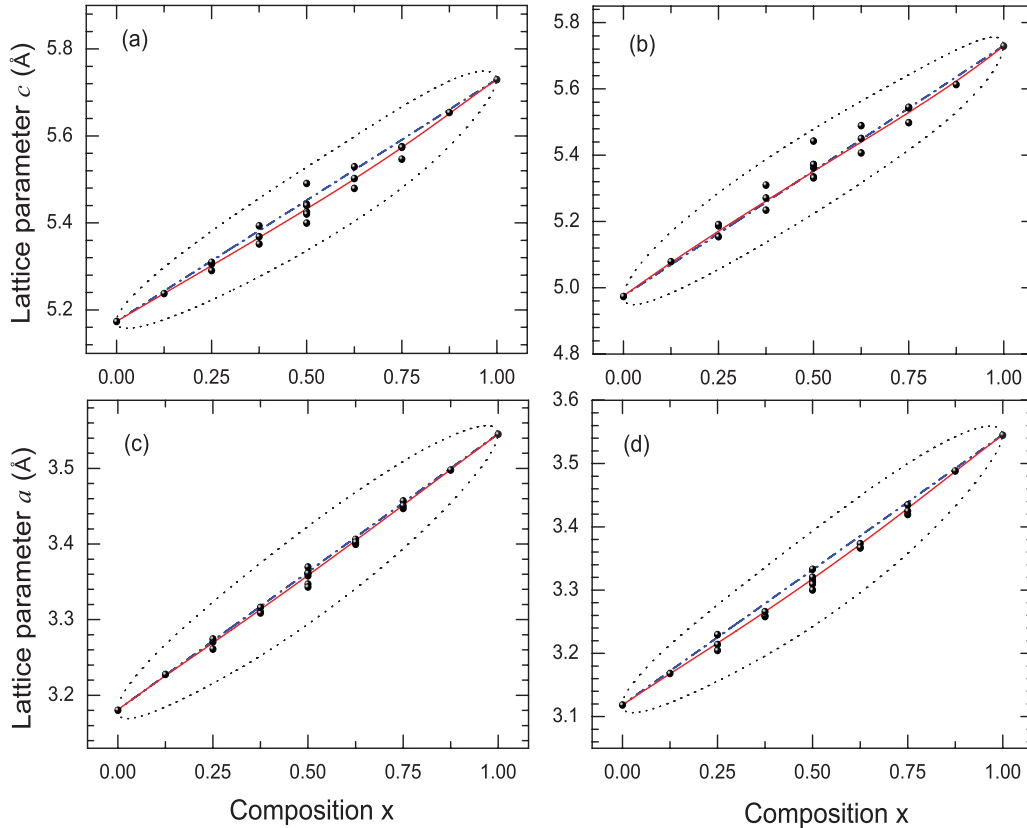FIG. 5. (Color online) Lattice parameters c [(a) and (b)] and a [(c) and (d)] of In$_x$Ga$_{1-x}$N [(a) and (c)] and In$_x$Al$_{1-x}$N [(b) and (d)] alloys in wz geometry versus composition x for the MDM (dot-dashed blue line) and the SRS statistics (red solid line). The black dotted lines indicate the mean-square deviations within SRS. The dots represent the results versus the fraction $n_j/8$ of the individual cluster materials.

that tetrahedra N-In$_2$X$_2$ exhibit the strongest deviations from the ideal situation due to the high lattice mismatches between InN-AlN and InN-GaN.

Figure 6 depicts the configurational averages for the bulk moduli of In$_x$Ga$_{1-x}$N and In$_x$Al$_{1-x}$N as obtained within the MDM and the SRS model. As for the lattice parameters, the SRS model leads to deviations of the elastic properties from the linear interpolation. The composition-*independent* bowing parameters amount to $B_b = 0.88/2.19$ GPa for In$_x$Ga$_{1-x}$N/In$_x$Al$_{1-x}$N. In addition, Fig. 6 shows that the strongest deviations of B_0 from the linear interpolation occur in the composition range $0 < x \leqslant 0.5$. They mainly follow the deviation of the lattice parameter a, as can be seen from a comparison with Fig. 5.

IV. ELECTRONIC PROPERTIES

A. Energy zero and alignment

For each of the 22 cluster classes of the In$_x$Ga$_{1-x}$N and In$_x$Al$_{1-x}$N alloys, the QP band structure is calculated using the HSE06+G_0W_0 method. However, the definition of an average band structure for a given composition x and its calculation by means of the Connolly-Williams formula,[46] Eq. (1), is difficult[71] because the energy zeros of the cluster classes are different and the size of the BZ varies from class to class. However, for energies at the Γ point such an average is possible since the symmetries of the corresponding energy

states can be related to each other. This holds, for example, for the energies of the lowest conduction-band state E_{c_j} and highest valence-band state E_{v_j}.

The configurational average Eq. (1) is however possible for the density of states (DOS) after alignment of the individual energy scales. When comparing single-QP energies of different cluster materials j one has to consider a common absolute energy scale (i.e., an internal reference level to which the individual QP energy scales of the individual cluster classes can be aligned). The space-averaged electrostatic potential (or sometimes the total KS potential) can provide such a level of reference. Alternatively, deep (atomic) levels such as the semicore d states can be used for the alignment.

In this work, we pursue an approach which relies on the picture of Fermi-level pinning; in this case the natural level of reference for the QP energies is the branch-point energy (BPE).[72–77] At the BPE the electronic states change their character from predominantly acceptorlike (usually valence states) to donorlike (usually conduction states). Therefore, it is assumed that the global Fermi level of the electrons is pinned near the BPE. Here, the BPEs are computed for each cluster material using a modified Tersoff approach[77] taking the lowest eight conduction bands and the highest 16 valence bands into account. The computed BPEs (cf. Table I) indicate that the branch point is located in the conduction bands for In-rich clusters up to about $n_j = 5$ ($n_j = 4$) for In$_{n_j}$Ga$_{8-n_j}$N$_8$ (In$_{n_j}$Al$_{8-n_j}$N$_8$).
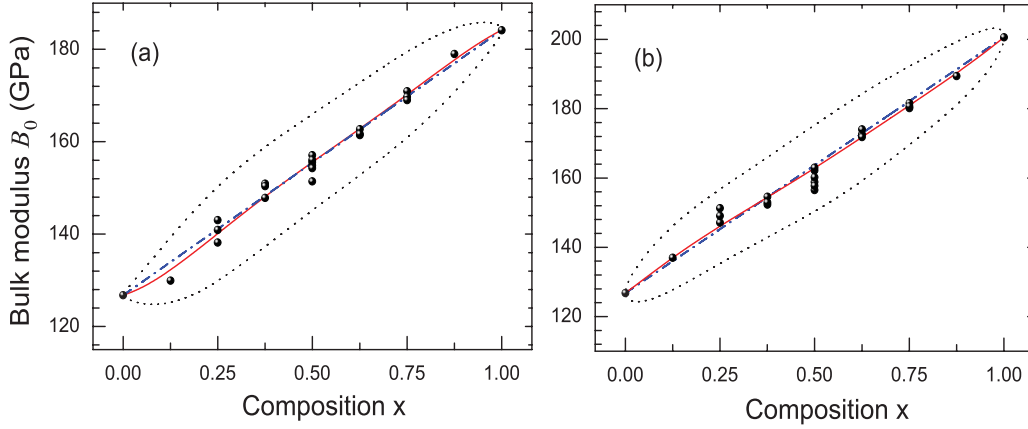
FIG. 6. (Color online) Bulk modulus B_0 of $In_xGa_{1-x}N$ (a) and $In_xAl_{1-x}N$ (b) alloys in wz geometry versus composition x computed using the MDM (dot-dashed blue line) and the SRS statistics (red solid line). The black dotted lines indicate the mean-square deviations within the SRS model. The dots represent the bulk moduli of the individual clusters.

B. Density of states

The calculated QP electronic structures lead to significantly different DOSs of the individual cluster materials. Some features of the individual clusters remain conserved in an alloy. The strongly dispersive conduction band found for the nitrides, in particular for InN, leads to a slowly increasing tail of the density of the conduction-band states. Since all clusters contribute within the SRS model, the configurational averages of these tails render a definition of the band edges $E_c(x)$ and $E_v(x)$ very difficult (see Fig. 7). Therefore, we added lines to Fig. 7 to indicate where the Lorenzian-broadened DOS of the occupied and empty states becomes smaller than 0.01 (eV·pair)$^{-1}$. These lines provide insight into the composition dependence of the conduction-band and valence-band edges in the mixed crystals. Interestingly, they indicate for $E_c(x)$ at intermediate compositions x that clusters with a fundamental gap $E_{g,j}$ (cf. Table I) close to the one of InN significantly contribute to the alloy. The DOS differences between the GaN [(a) and (b)] and AlN [(c) and (d)] containing alloys are not only visible in the gap regions but also for low energies due to the occurrence of Ga $3d$ states.

Figure 7 also depicts the influence of the cluster statistics on the composition dependence of $E_c(x)$ and $E_v(x)$: While the MDM leads to a linear transition between the binary end components, the SRS statistics yields a significant nonlinearity. In the case of the SRS model the DOS of all the cluster materials contribute to the peaks which is visible especially in the conduction-band region, where the DOS for intermediate compositions x significantly differs from the one of the binary end components. In the case of the MDM the linear transition between the DOSs of the binary end components is visible and mainly affects the heights of the peaks. The lower part of the uppermost p-like valence band region also differs significantly between the two statistics for both alloys. This striking difference in the composition dependence should be useful for the characterization of the cluster statistics and distribution by means of spectroscopic methods such as the investigation of the occupied DOS by means of x-ray photoemission (see, e.g., Ref. 78).

C. Quasiparticle energies around the band edges

In Fig. 8(a) the QP energies of the lowest conduction-band level, $E_{c,j}$, and of the highest valence-band level, $E_{v,j}$, are plotted for all cluster classes of the $In_xGa_{1-x}N$ and $In_xAl_{1-x}N$ alloys. In addition, the respective configurational averages, $E_c(x)$ and $E_v(x)$, as calculated within the SRS model, are shown. This figure indicates a nonlinear variation of the band edges with the composition x of the alloys. It also shows that the gaps of the different cluster classes, that have the same number of In cations, vary significantly. More specifically, this variation can be on the same order of magnitude as the change that is observed when increasing or decreasing the number of In cations by one [see, e.g., $x = 0.25$ or $x = 0.5$ in Fig. 8(a)].

In the light of the cluster ordering, for a given n_j we find that the energetically most unfavorable clusters with the strongest ordering (i.e., the highest tendency D_j for clustering) give rise to the smallest energy distances $E_{g,j} = E_{c,j} - E_{v,j}$. This observation, which is in agreement with other theoretical studies,[24] becomes clear, for instance, for $j = 2$ or $j = 19$ in comparison to classes 3, 4 or 17, 18: In both cases the clusters are ordered ($D_j = 0.5$) with the same type of cations in c planes with alternating bilayers. In addition, these cluster materials have the lowest conduction-band and highest valence-band states of all clusters for fixed $n_j = 2$ or $n_j = 6$, respectively. For $n_j = 4$ the situation is similar. The classes $j = 8, 9$, and 11 with $D_j = 1.0$ yield the smallest gaps.

The top of valence-band states is studied in Fig. 8(b) in more detail. The three uppermost valence states are depicted versus the cluster fraction $n_j/8$ for each cluster class. Their average values using the SRS statistics versus the average composition x are also shown, despite the difficulties in identifying the symmetry of the states due to the cation-site occupation and atomic relaxation. An additional problem appears in the $In_xAl_{1-x}N$ case. For the binary end components these states possess Γ_5 and Γ_1 symmetry (wz-InN and wz-GaN) or Γ_1 and Γ_5 symmetry (wz-AlN).[79] The reason for the different ordering of the valence-band symmetries is the sign of the crystal-field splitting: It is positive (35.6 meV for InN and 28.5 meV for GaN) for the two nitrides with d electrons, but
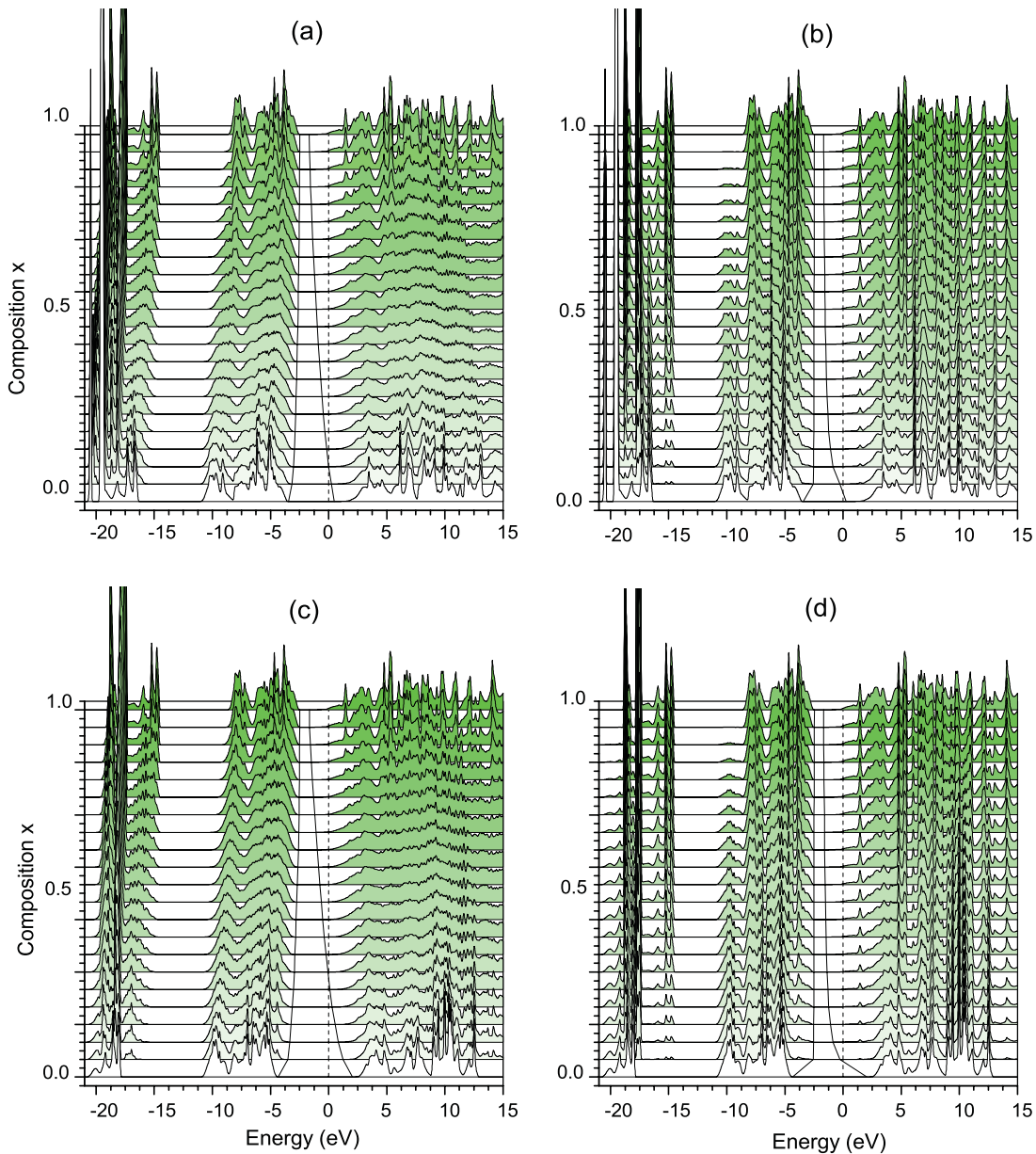
FIG. 7. (Color online) DOS in (eV·pair)$^{-1}$ (green areas) of the In$_x$Ga$_{1-x}$N [(a) and (b)] and In$_x$Al$_{1-x}$N [(c) and (d)] alloys versus energy (in eV), as a function of the composition x. The BPE has been used as energy zero (black dashed line). The curves are calculated as configurational averages using the cluster fractions from the SRS model [(a) and (c)] or the MDM [(b) and (d)]. The DOS of the binary end components is shown for the compositions $x = 0.0$ and $x = 1.0$. The Lorentzian broadening parameter amounts to 0.1 eV. In addition, as a guide to the eye (see text), the black solid lines indicate where the DOS in the gap region decreases to 0.01 (eV·pair)$^{-1}$.

negative (-275.8 meV) for AlN. As a consequence of this change of the band ordering, the levels in In$_x$Al$_{1-x}$N will cross at a certain fraction $n_j/8$ or composition x in order to guarantee the different signs of the crystal-field splitting. However, the situation is even more complicated, since for the cluster classes $0 < j < 21$ the symmetry of the atomic basis is significantly reduced. Therefore, the uppermost valence levels do not have the Γ_5 or Γ_1 symmetries. For these reasons it is difficult to describe the evolution of the Γ_5 and Γ_1 levels for varying compositions x and we pursue an approximate approach instead: In the case of In$_x$Ga$_{1-x}$N we assume the same energetic ordering of the levels as found for GaN

and InN. This procedure leads to the three lines plotted in Fig. 8(b). Instead, in the case of In$_x$Al$_{1-x}$N the ordering shown in Fig. 8(b) is only true for $x \to 0$ and $x \to 1$, since we have *assumed* the crossing of the Γ_5 and Γ_1 levels to occur between $x = 0.125$ and $x = 0.25$.

D. Fundamental gap and bowing

In Fig. 9, the results for the fundamental band gaps $E_{g,j}$ (cf. Table I) of all cluster materials are depicted together with the configurational averages $E_g(x)$ as a function of the composition x for both alloys. As discussed for the highest
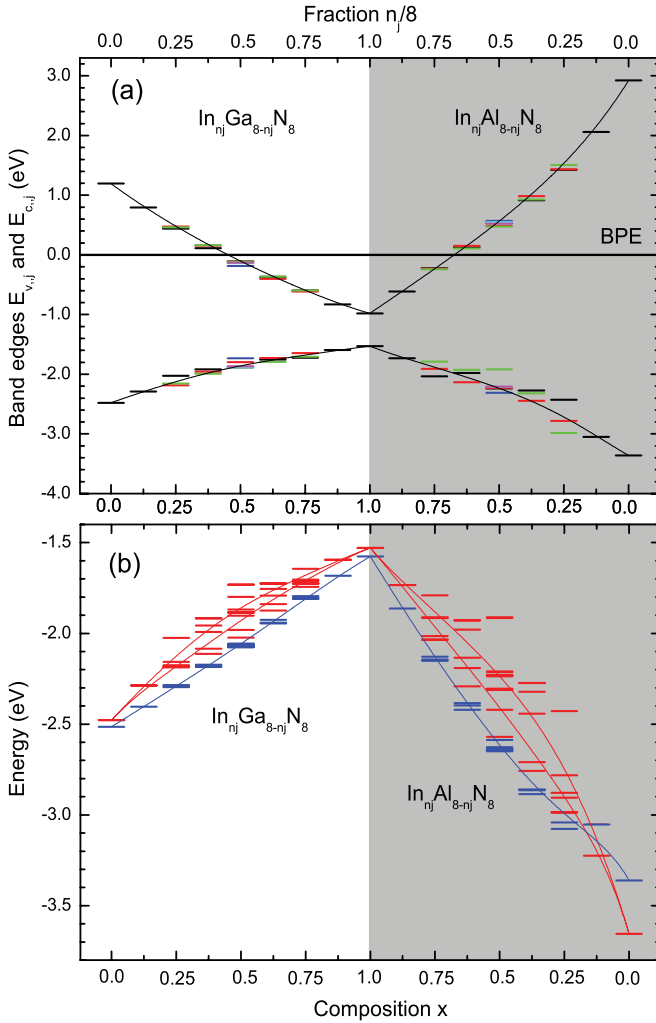
FIG. 8. (Color online) QP energy levels around the fundamental band gap for each cluster class j. In (a) the lowest conduction-band ($E_{c,j}$) and the highest valence-band ($E_{v,j}$) states are plotted. In (b) the two uppermost valence levels at the Γ point are shown as calculated for each cluster j in the HSE06+G_0W_0 approximation. For the binary end components in the wz structure these states are of Γ_5 (red) or Γ_1 (blue) type. The twofold degeneracy of the Γ_5 levels is lifted due to the deviations from the C_{6v}^4 symmetry at intermediate compositions. The configurational averages resulting within the SRS statistics are shown as a guide to the eyes. The BPE has been used as energy zero.

total energy (cf. Sec. III A), there is also a correlation of the fundamental band gap with the vertical ordering of the In and the Ga/Al atoms along the c axis: The lowest gap appears for the highest degree of ordering $D_j = 1$ for $n_j = 4$. In the case of the ordered geometries, such as the $(InN)_1(XN)_1(0001)$ superlattices (see discussion above), the majority of In-N and X-N bonds are practically unstrained. These In-N bonds lead to a lowering of the gap in the cluster material toward the value of bulk InN.

As shown in Fig. 9, the gaps of the individual cluster materials clearly indicate a strongly nonlinear variation with the composition. Consequently, the composition-*independent* bowing parameters [cf. Eq. (7)] obtained within the SRS statistics amount to $E_{g,b} = 1.57$ eV ($In_xGa_{1-x}N$) and $E_{g,b} = 3.03$ eV ($In_xAl_{1-x}N$). The physics underlying to the bowing
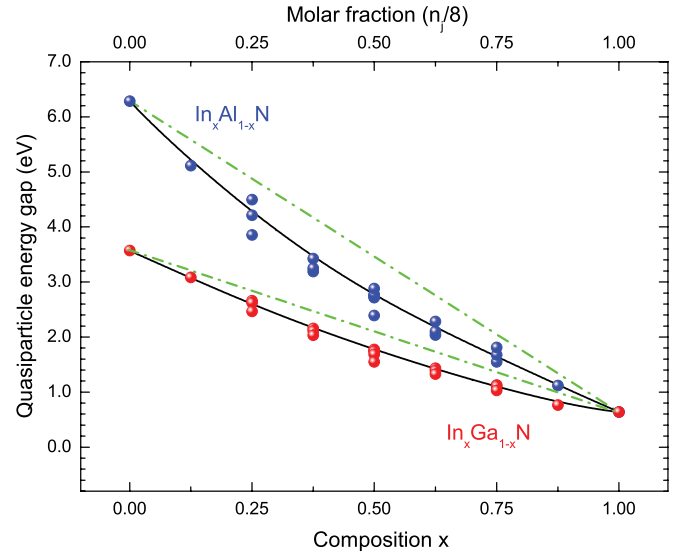
FIG. 9. (Color online) Quasiparticle energy gap of $In_xGa_{1-x}N$ and $In_xAl_{1-x}N$ alloys in wz geometry versus composition x as computed using the MDM (dot-dashed green line) and the SRS model (black solid line). The dots represent the band gaps of the individual clusters.

parameter has been discussed in detail elsewhere.[80,81] When a possible composition dependence of the bowing parameter is taken into account [cf. Eq. (8)], we obtain $E_{g,b_0} = 1.42\,(2.24)$ eV and $E_{g,b_1} = -0.348\,(-0.875)$ for $In_xGa_{1-x}N$ ($In_xAl_{1-x}N$). These numbers for the composition-dependent bowing parameters $E_{g,b}$ indicate a stronger bowing for InN-rich alloys in comparison to the XN-rich alloys.

Comparing the bowing parameters calculated in this work to results computed by other authors (see Refs. 21,24,32, and 82 and references therein) shows the same order of magnitude. Vurgaftman *et al.*[4] recommend values of $E_{g,b} = 1.4$ eV ($In_xGa_{1-x}N$) and $E_{g,b} = 2.5$ eV ($In_xAl_{1-x}N$) which are close to the ones predicted in this work. The calculated results slightly overestimate the experimental ones, which can be the consequence of the fact that the SRS model gives an upper limit for the bowing. The deviation of experimental parameters for $In_xAl_{1-x}N$ may also be traced back to the use of only AlN-rich samples.[48]

In addition, Fig. 9 shows that clustering can lead to a substantial increase of the bowing,[24] especially for $In_xAl_{1-x}N$: Several gap values $E_{g,j}$ appear below the configurational average obtained within the SRS model. Assuming that the cluster material which has the smallest gap for $n_j = 4$ ($E_{g,j} = 1.644$ eV for $In_4Ga_4N_8$ and $E_{g,j} = 2.571$ eV for $In_4Al_4N_8$) determines the alloy properties at $x = 0.5$, we obtain increased bowing parameters of 1.84 eV ($In_xGa_{1-x}N$) and 3.65 eV ($In_xAl_{1-x}N$). However, these values are still smaller than those predicted by Gorczyca *et al.*[24] for the "clustering" scenario. In any case, the significant bowing of the gap found in experiment and in the calculations shows that a linear interpolation is not valid for both alloys.

In Fig. 10, the configurational averages for the band gaps are compared to optically measured results for $In_xGa_{1-x}N$ and $In_xAl_{1-x}N$. For both alloys, most of the measured gap values
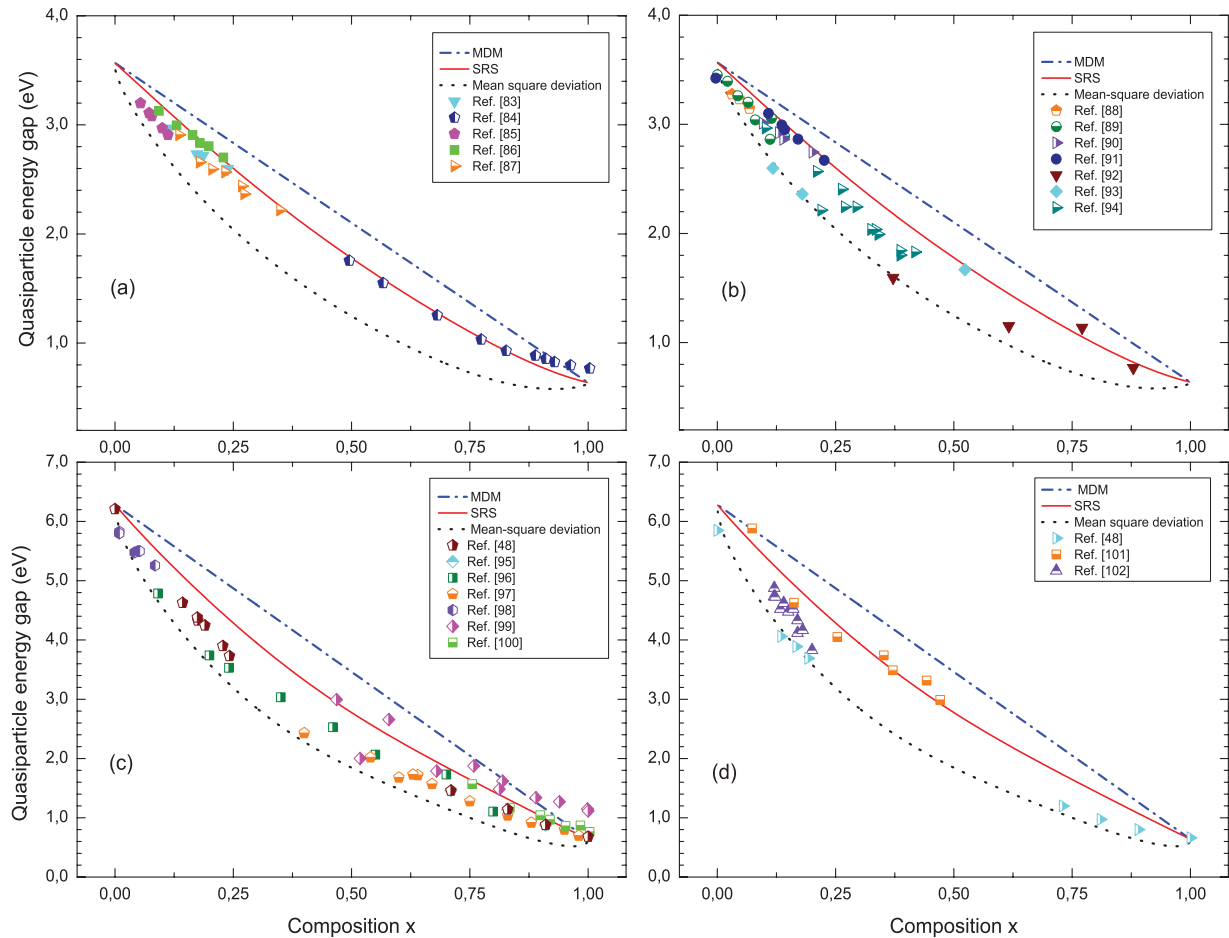
FIG. 10. (Color online) Quasiparticle energy gaps of In$_x$Ga$_{1-x}$N [(a) and (b)] and In$_x$Al$_{1-x}$N [(c) and (d)] alloys in *wz* geometry versus composition *x* computed using the MDM (dot-dashed blue line) and the SRS model (red solid line). The black dotted line describes the band gap reduced by the mean-square deviation, $E_g(x) - \Delta E_g(x)$. In panels (a) and (c) we compare with absorption data (different symbols) while the experimental gaps (different symbols) in panels (b) and (d) have been derived from luminescence measurements: (a) Refs. 83–87, (b) Refs. 88–94, (c) Refs. 48,95–100, and (d) Refs. 48,101, and 102.

appear within $E_g(x)$ and $E_g(x) - \Delta E_g(x)$ (i.e., the configurational average reduced by the mean-square deviation). The few exceptions (e.g., the absorption measurements of Wu *et al.*[84] or the values derived by Naoi *et al.*[99]) for InN-rich In$_x$Ga$_{1-x}$N alloys, however, approach (for $x \to 1$) a gap which is larger than the theoretical gap of $E_g = 0.64$ eV computed for InN within this work.

For a more detailed comparison, we divide the measured data into two groups: In Figs. 10(a) and 10(c) we compare to results derived from absorption measurements and in Figs. 10(b) and 10(d) energies obtained from photoluminescence are used. Therefore, we claim that extrapolating the absorption edge in a random alloy to the limit of vanishing absorption defines an average gap of the system. The absorption onset can be affected by larger regions of the alloy, hence, it is better represented by the configurationally averaged band gaps. Contrary, in the case of the photoluminescence or cathode luminescence, the excited electron-hole pairs diffuse and relax until they reach domains with the smallest *local* gaps as long as the time constants for diffusion and relaxation are smaller than the lifetime of the excited electron-hole pairs. Consequently, the luminescence results should not be compared to $E_g(x)$, but to

$E_g(x) - \Delta E_g(x)$ instead (i.e., to the configurational average reduced by the mean-square deviation).

The comparison of $E_g(x)$ to absorption data [cf. Fig. 10(a)] suggests that the SRS model seems to correctly describe the dependence of the measured absorption onsets on the average composition *x* for In$_x$Ga$_{1-x}$N. Especially the values of Nakamura *et al.*[86] are in good agreement. The results of McCluskey *et al.*[85] and O'Donnell *et al.*[87] indicate a deviation of $E_g(x)$ toward $E_g(x) - \Delta E_g(x)$ which may be a consequence of stronger composition fluctuations in the samples. This trend is found to be more pronounced for absorption studies of In$_x$Al$_{1-x}$N [cf. Fig. 10(c)] which might be related to larger composition fluctuations due to the increased internal strain caused by the bigger bond-length difference between In-N and Al-N in comparison to Ga-N. Ordered structures play a less important role since their gap values are closer to the $E_g(x)$ curve than the measured values.

The physical picture derived from the luminescence measurements is less clear. For In$_x$Ga$_{1-x}$N [cf. Fig. 10(b)] the experimental points are further away from the $E_g(x)$ curve than the ones in Fig. 10(a). However, only a few measurements (e.g., those of Davydov *et al.*[92] and Kim *et al.*[93]) follow

the $E_g(x) - \Delta E_g(x)$ line. Deviations found in other measurements may be a consequence of the actual alloy samples with local appearance of ordered structures and/or composition fluctuations. Measured values for $In_xAl_{1-x}N$ [cf. Fig. 10(d)] can be described by $E_g(x)$ (those of Onuma *et al.*[102]) as well as $E_g(x) - \Delta E_g(x)$ (those of Sakalauskas *et al.*[48]). The ones by Carlin *et al.*[101] are in between the two theoretical curves. The mean-square deviations computed within the SRS statistics seem to describe an upper limit for the difference in the absorption onset and the luminescence line. This difference is usually identified with the Stokes shift, but it is caused by the chemical (and partly structural) disorder in this work.[81]

Taking the mean-square deviation [cf. Eq. (2)] for the fundamental band gaps into account can increase the bowing from 1.6 eV (see above) to 3.6 eV ($In_xGa_{1-x}N$) or from 3.0 eV (see above) to 7.5 eV ($In_xAl_{1-x}N$) when going from $E_g(x)$ to $E_g(x) - \Delta E_g(x)$. These results indicate that the wide spread of bowing parameters found in the literature can be related to the different experimental methods and preparation techniques. Interestingly, our actual bowing-parameter values are almost embedded by values of 1.7–2.8 eV / 2.5–6.5 eV ($In_xGa_{1-x}N$) or 2.1–6.2 eV / 3.9–14 eV ($In_xAl_{1-x}N$) computed by Gorczyca *et al.*[24] assuming a more uniform/clustered distribution of the In atoms.

V. SUMMARY AND CONCLUSIONS

The structural and electronic properties of *wz*-derived $In_xGa_{1-x}N$ and $In_xAl_{1-x}N$ alloys are calculated using a cluster expansion approach together with two different cluster statistics (i.e., the strict-regular solution and the microscopic decomposition model). The total-energy optimizations are performed within density functional theory using the gradient-corrected AM05 XC functional. In order to obtain the electronic structures, a recently developed quasiparticle method, based on the hybrid HSE06 XC functional and subsequent G_0W_0 corrections, is used. The branch-point energies of all individual clusters are used to align the quasiparticle energies of all clusters on a common energy scale.

We find that the cluster materials that are structurally ordered (mostly in *c*-axis direction) are energetically less favorable. The lowest energies are computed for the cluster classes with a high tendency for clustering (i.e., large deviation

of the actual cation-site occupation of the tetrahedra from the average value $n_j/2$ and, hence, $D_j \to 1$). The influence of the cluster statistics on the structural properties is rather weak and we conclude that the deviations from Vegard's rule are small but measurable, especially for $In_xAl_{1-x}N$. In the case of the bulk modulus, the deviations are slightly larger. Overall, the energetic, structural, and elastic properties of the alloys are less sensitive to the details of the local distribution of the cations.

The electronic properties, however, are much more sensitive to the distribution of the cations over the alloy. For the two cluster statistics used in this work, the variation of the quasiparticle DOS (peak positions as well as peak intensities) with the composition x is completely different. Composition-dependent band edges as well as the positions of the three uppermost valence bands at the Γ point (along with their splittings) are derived. In this context, the difficulties that arise from the lower symmetry of the clusters with intermediate compositions as well as from the different band ordering in InN and AlN, are discussed.

Comparing the calculated energy gaps to measured data clearly shows that the strict-regular solution statistics seems to yield a more realistic picture than the macroscopic decomposition model. Since the large variety of results for band gaps from optical measurements falls between the curves for the average gap $E_g(x)$ and the one reduced by the mean-square deviation, $E_g(x) - \Delta E_g(x)$, we conclude that composition fluctuations in the alloys play an important role. The measured absorption onsets appears close to $E_g(x)$, whereas the luminescence data approaches $E_g(x) - \Delta E_g(x)$. This fact is in agreement with the picture that excited electron-hole pairs prefer to radiatively recombine in the domains of the alloy that have the lowest band gap.

*luiz-claudio.de-carvalho@uni-jena.de

[1]J. Wu, J. Appl. Phys. **106**, 011101 (2009).

[2]V. Davydov, A. Klochikhin, V. Emtsev, D. Kurdyukov, S. Ivanov, V. Vekshin, F. Bechstedt, J. Furthmüller, J. Aderhold, J. Graul, A. Mudryi, H. Harima, A. Hashimoto, A. Yamamoto, and E. E. Haller, Phys. Status Solidi B **234**, 787 (2002).

[3]J. Wu, W. Walukiewicz, K. M. Yu, J. W. Ager III, E. E. Haller, H. Lu, W. J. Schaff, Y. Saito, and Y. Nanishi, Appl. Phys. Lett. **80**, 3967 (2002).

[4]I. Vurgaftman and J. R. Meyer, J. Appl. Phys. **94**, 3675 (2003).

[5]J. Phillips, M. Coltrin, M. Crawford, A. Fischer, M. Krames, R. Mueller-Mach, G. Mueller, Y. Ohno, L. Rohwer, J. Simmons, and J. Tsao, Laser & Photon. Rev. **1**, 307 (2007).

[6]F. Yam and Z. Hassan, Superlattices Microstruct. **43**, 1 (2008).

[7]T. Nagatomo, T. Kuboyama, H. Minamino, and O. Omoto, Jpn. J. Appl. Phys. **28**, L1334 (1989).

[8]N. Yoshimoto, T. Matsuoka, T. Sasaki, and A. Katsui, Appl. Phys. Lett. **59**, 2251 (1991).

[9]I.-H. Ho and G. B. Stringfellow, Appl. Phys. Lett. **69**, 2701 (1996).

[10]G. Popovici and H. Morkoç, in *GaN and Related Materials II* (Gordon and Breach Science, Amsterdam, 2000), pp. 93–172.

[11]P. Ruterana, G. Nouet, W. Van der Stricht, I. Moerman, and L. Considine, Appl. Phys. Lett. **72**, 1742 (1998).

[12]D. Doppalapudi, S. N. Basu, K. F. J. Ludwig, and T. D. Moustakas, J. Appl. Phys. **84**, 1389 (1998).

[13]N. A. El-Masry, E. L. Piner, S. X. Liu, and S. M. Bedair, Appl. Phys. Lett. **72**, 40 (1998).

[14]M. D. McCluskey, L. T. Romano, B. S. Krusor, D. P. Bour, N. M. Johnson, and S. Brennan, Appl. Phys. Lett. **72**, 1730 (1998).

[15]E. Zielinska-Rohozanska, J. Gronkowski, M. Regulska, M. Majer, and K. Pakula, Cryst. Res. Technol. **36**, 903 (2001).

[16]Z. Liliental-Weber, D. Zakharov, K. Yu, J. Ager III, W. Walukiewicz, E. Haller, H. Lu, and W. Schaff, Physica B: Condensed Matter **376**, 468 (2006).

[17]P. Ruterana, S. Kret, A. Vivet, G. Maciejewski, and P. Dluzewski, J. Appl. Phys. **91**, 8979 (2002).

[18]T. M. Smeeton, M. J. Kappers, J. S. Barnard, M. E. Vickers, and C. J. Humphreys, Appl. Phys. Lett. **83**, 5419 (2003).

[19]S. F. Chichibu, A. Uedono, T. Onuma, B. A. Haskell, A. Chakraborty, T. Koyama, P. T. Fini, S. Keller, S. P. Denbaars, J. S. Speck, U. K. Mishra, S. Nakamura, S. Yamaguchi, S. Kamiyama, H. Amano, I. Akasaki, J. Han, and T. Sota, Philos. Mag. **87**, 2019 (2007).

[20]A. Wakahara, T. Tokuda, X.-Z. Dang, S. Noda, and A. Sasaki, Appl. Phys. Lett. **71**, 906 (1997).

[21]L. K. Teles, J. Furthmüller, L. M. R. Scolfaro, J. R. Leite, and F. Bechstedt, Phys. Rev. B **62**, 2475 (2000).

[22]F. Grosse and J. Neugebauer, Phys. Rev. B **63**, 085207 (2001).

[23]M. G. Ganchenkova, V. A. Borodin, K. Laaksonen, and R. M. Nieminen, Phys. Rev. B **77**, 075207 (2008).

[24]I. Gorczyca, S. P. Łepkowski, T. Suski, N. E. Christensen, and A. Svane, Phys. Rev. B **80**, 075202 (2009).

[25]J. A. Chan, J. Z. Liu, and A. Zunger, Phys. Rev. B **82**, 045112 (2010).

[26]J. Z. Liu and A. Zunger, Phys. Rev. B **77**, 205201 (2008).

[27]C. K. Gan, Y. P. Feng, and D. J. Srolovitz, Phys. Rev. B **73**, 235214 (2006).

[28]S. Nakamura and G. Fasol, *The Blue Laser Diode: GaN Based Light Emitters and Lasers* (Springer, Berlin, 1997).

[29]S. Chichibu, T. Azuhata, T. Sota, and S. Nakamura, Appl. Phys. Lett. **70**, 2822 (1997).

[30]S. F. Chichibu, A. Uedono, T. Onuma, B. A. Haskell, A. Chakraborty, T. Koyama, P. T. Fini, S. Keller, S. P. DenBaars, J. S. Speck, U. K. Mishra, S. Nakamura, S. Yamaguchi, S. Kamiyama, H. Amano, I. Akasaki, and J. a. Han, Nat. Mater. **5**, 810 (2006).

[31]L. K. Teles, L. M. R. Scolfaro, J. R. Leite, J. J. Furthmüller, and F. Bechstedt, J. Appl. Phys. **92**, 7109 (2002).

[32]M. Ferhat and F. Bechstedt, Phys. Rev. B **65**, 075213 (2002).

[33]M. Marques, L. K. Teles, L. M. R. Scolfaro, J. R. Leite, J. Furthmüller, and F. Bechstedt, Appl. Phys. Lett. **83**, 890 (2003).

[34]P. G. Moses and C. G. V. de Walle, Appl. Phys. Lett. **96**, 021908 (2010).

[35]R. R. Pela, C. Caetano, M. Marques, L. G. Ferreira, J. Furthmüller, and L. K. Teles, Appl. Phys. Lett. **98**, 151907 (2011).

[36]P. Hohenberg and W. Kohn, Phys. Rev. **136**, B864 (1964).

[37]W. Kohn and L. J. Sham, Phys. Rev. **140**, A1133 (1965).

[38]W. G. Aulbur, L. Jönsson, and J. W. Wilkins, in *Advances in Research and Applications*, Solid State Physics, Vol. 54, edited by H. Ehrenreich and F. Spaepen (Academic Press, San Diego, 1999), pp. 1–218.

[39]A. Schleife, C. Rödl, J. Furthmüller, and F. Bechstedt, New J. Phys. **13**, 085012 (2011).

[40]C. Caetano, L. K. Teles, M. Marques, A. Dal Pino, and L. G. Ferreira, Phys. Rev. B **74**, 045215 (2006).

[41]A. Zunger, in *Statistics and Dynamics of Alloy Phase Transformations*, edited by P. E. A. Turchi and A. Gonis (Plenum Press, New York, 1994), p. 361.

[42]S.-H. Wei, L. G. Ferreira, and A. Zunger, Phys. Rev. B **41**, 8240 (1990).

[43]A. Schleife, M. Eisenacher, C. Rödl, F. Fuchs, J. Furthmüller, and F. Bechstedt, Phys. Rev. B **81**, 245210 (2010).

[44]A. Sher, M. van Schilfgaarde, A.-B. Chen, and W. Chen, Phys. Rev. B **36**, 4279 (1987).

[45]A.-B. Chen and A. Sher, *Semiconductor Alloys* (Plenum, New York, 1995).

[46]J. W. D. Connolly and A. R. Williams, Phys. Rev. B **27**, 5169 (1983).

[47]L. Vegard, Z. Phys. **5**, 17 (1921).

[48]E. Sakalauskas, H. Behmenburg, C. Hums, P. Schley, G. Rossbach, C. Giesen, M. Heuken, H. Kalisch, R. H. Jansen, J. Bläsing, A. Dadgar, A. Krost, and R. Goldhahn, J. Phys. D: Appl. Phys. **43**, 365102 (2010).

[49]R. Armiento and A. E. Mattsson, Phys. Rev. B **72**, 085108 (2005).

[50]G. Kresse and J. Furthmüller, Phys. Rev. B **54**, 11169 (1996).

[51]G. Kresse and D. Joubert, Phys. Rev. B **59**, 1758 (1999).

[52]H. J. Monkhorst and J. D. Pack, Phys. Rev. B **13**, 5188 (1976).

[53]F. D. Murnaghan, Proc. Nat. Acad. Sci. USA **30**, 244 (1944).

[54]G. Onida, L. Reining, and A. Rubio, Rev. Mod. Phys. **74**, 601 (2002).

[55]L. Hedin and S. Lundqvist, Solid State Phys. **23**, 1 (1969).

[56]F. Fuchs, J. Furthmüller, F. Bechstedt, M. Shishkin, and G. Kresse, Phys. Rev. B **76**, 115109 (2007).

[57]J. Heyd, G. E. Scuseria, and M. Ernzerhof, J. Chem. Phys. **124**, 219906 (2006).

[58]F. Bechstedt, F. Fuchs, and G. Kresse, Phys. Status Solidi B **246**, 1877 (2009).

[59]J. Paier, M. Marsman, K. Hummer, G. Kresse, I. C. Gerber, and J. G. Ángyán, J. Chem. Phys. **124**, 154709 (2006).

[60]J. Paier, M. Marsman, K. Hummer, G. Kresse, I. C. Gerber, and J. G. Ángyán, J. Chem. Phys. **125**, 249901 (2006).

[61]L. C. de Carvalho, A. Schleife, and F. Bechstedt, Phys. Rev. B **84**, 195105 (2011).

[62]J. M. Cowley, J. Appl. Phys. **21**, 24 (1950).

[63]M. Lopuszyński and J. Majewski, Phys. Rev. B **85**, 035211 (2012).

[64]M. Sanati, G. L. W. Hart, and A. Zunger, Phys. Rev. B **68**, 155210 (2003).

[65]J. Adhikari and D. A. Kofke, J. Appl. Phys. **95**, 6129 (2004).

[66]A. Zunger and S. Mahajan, in *Handbook on Semiconductors*, edited by S. Mahajan (North-Holland, Amsterdam, 1994), Vol. 3, Chap. 19, p. 1399.

[67]A. F. Wright and J. S. Nelson, Phys. Rev. B **51**, 7866 (1995).

[68]H. Schulz and K. H. Thiemann, Solid State Commun. **23**, 815 (1977).

[69]K. Osamura, J. Appl. Phys. **46**, 3432 (1975).

[70]L. Vegard, Z. Phys. **5**, 17 (1921).

[71]V. Popescu and A. Zunger, Phys. Rev. Lett. **104**, 236403 (2010).

[72]A. Belabbes, L. C. de Carvalho, A. Schleife, and F. Bechstedt, Phys. Rev. B **84**, 125108 (2011).

[73]W. Mönch, *Semiconductor Surfaces and Interfaces* (Springer, Berlin, 2001).

[74]F. Flores and C. Tejedor, J. Phys. C **12**, 731 (1979).

[75] J. Tersoff, Phys. Rev. B **30**, 4874 (1984).

[76] C. Tejedor and F. Flores, J. Phys. C **11**, L19 (1977).

[77] A. Schleife, F. Fuchs, C. Rödl, J. Furthmüller, and F. Bechstedt, Appl. Phys. Lett. **94**, 012104 (2009).

[78] P. D. C. King, T. D. Veal, C. F. McConville, C. F. Fuchs, J. Furthmüller, F. Bechstedt, J. Schörmann, D. J. As, K. Lischka, H. Lu, and W. J. Schaff, Phys. Rev. B **77**, 115213 (2008).

[79] L. C. de Carvalho, A. Schleife, F. Fuchs, and F. Bechstedt, Appl. Phys. Lett. **97**, 232101 (2010).

[80] I. Gorczyca, T. Suski, N. E. Christensen, and A. Svane, Phys. Rev. B **83**, 153301 (2011).

[81] M. Ferhat, J. Furthmüller, and F. Bechstedt, Appl. Phys. Lett. **80**, 1394 (2002).

[82] L. G. Ferreira, M. Marques, and L. K. Teles, Phys. Rev. B **78**, 125116 (2008).

[83] S. Pereira, M. R. Correia, T. Monteiro, E. Pereira, E. Alves, A. D. Sequeira, and N. Franco, Appl. Phys. Lett. **78**, 2137 (2001).

[84] J. Wu, W. Walukiewicz, W. Shan, K. M. Yu, J. W. Ager, E. E. Haller, H. Lu, and W. J. Schaff, Phys. Rev. B **66**, 201403 (2002).

[85] M. D. McCluskey, C. G. V. de Walle, L. T. Romano, B. S. Krusor, and N. M. Johnson, J. Appl. Phys. **93**, 4340 (2003).

[86] S. Nakamura, *Highlights in Condensed Matter Physics and Materials Science*, Solid Stat. Commun. **102**, 237 (1997).

[87] K. P. O'Donnell, I. Fernandez-Torrente, P. R. Edwards, and R. W. Martin, *Proceedings of the First ONR International Indium Nitride Workshop*, J. Cryst. Growth **269**, 100 (2004).

[88] F. Scholz, J. Off, A. Sohmer, V. Syganow, A. Dörnen, and O. Ambacher, J. Cryst. Growth **189-190**, 8 (1998).

[89] W. Shan, W. Walukiewicz, E. E. Haller, B. D. Little, J. J. Song, M. D. McCluskey, N. M. Johnson, Z. C. Feng, M. Schurman, and R. A. Stall, J. Appl. Phys. **84**, 4452 (1998).

[90] T. Takeuchi, H. Takeuchi, S. Sota, H. Sakai, H. Amano, and I. Akasaki, Jpn. J. Appl. Phys. **36**, L177 (1997).

[91] C. Wetzel, T. Takeuchi, S. Yamaguchi, H. Katoh, H. Amano, and I. Akasaki, Appl. Phys. Lett. **73**, 1994 (1998).

[92] V. Davydov, A. Klochikhin, V. Emtsev, S. Ivanov, V. Vekshin, F. Bechstedt, J. Furthmüller, H. Harima, A. Mudryi, A. Hashimoto, A. Yamamoto, J. Aderhold, J. Graul, and E. Haller, Phys. Status Solidi B **230**, R4 (2002).

[93] M.-H. Kim, J.-K. Cho, I.-H. Lee, and S.-J. Park, Phys. Status Solidi A **176**, 269 (1999).

[94] K. P. O'Donnell, J. F. W. Mosselmans, R. W. Martin, S. Pereira, and M. E. White, J. Phys.: Condens. Matter **13**, 6977 (2001).

[95] R. Goldhahn, P. Schley, A. Winzer, G. Gobsch, V. Cimalla, O. Ambacher, M. Rakel, C. Cobet, N. Esser, H. Lu, and W. Schaff, Phys. Status Solidi A **203**, 42 (2006).

[96] E. Iliopoulos, A. Adikimenakis, C. Giesen, M. Heuken, and A. Georgakilas, Appl. Phys. Lett. **92**, 191907 (2008).

[97] R. E. Jones, R. Broesler, K. M. Yu, J. W. Ager, E. E. Haller, W. Walukiewicz, X. Chen, and W. J. Schaff, J. Appl. Phys. **104**, 123501 (2008).

[98] K. S. Kim, A. Saxler, P. Kung, M. Razeghi, and K. Y. Lim, Appl. Phys. Lett. **71**, 800 (1997).

[99] H. Naoi, K. Fujiwara, S. Takado, M. Kurouchi, D. Muto, T. Araki, H. Na, and Y. Nanishi, J. Electron. Mater. **36**, 1313 (2007).

[100] W. Walukiewicz, S. X. Li, J. Wu, K. M. Yu, J. W. Ager, E. E. Haller, H. Lu, and W. J. Schaff, J. Cryst. Growth **269**, 119 (2004).

[101] J.-F. Carlin, C. Zellweger, J. Dorsaz, S. Nicolay, G. Christmann, E. Feltin, R. Butté, and N. Grandjean, Phys. Status Solidi B **242**, 2326 (2005).

[102] T. Onuma, S. Chichibu, Y. Uchinuma, T. Sota, S. Yamaguchi, S. Kamiyama, H. Amano, and I. Akasaki, J. Appl. Phys. **94**, 2449 (2003).